mater.scichina.com link.springer.com

Published online 29 July 2020 | https://doi.org/10.1007/s40843-020-1408-x
Sci China Mater 2021, 64(1): 52–60

Sn^{4+} precursor enables 12.4% efficient kesterite solar cell from DMSO solution with open circuit voltage deficit below 0.30 V

Yuancai Gong[1], Yifan Zhang[1], Erin Jedlicka[2], Rajiv Giridharagopal[2], James A. Clark[3], Weibo Yan[1], Chuanyou Niu[1], Ruichan Qiu[1], Jingjing Jiang[1], Shaotang Yu[1], Sanping Wu[1], Hugh W. Hillhouse[3], David S. Ginger[2], Wei Huang[1] and Hao Xin[1*]

ABSTRACT **The limiting factor preventing further performance improvement of the kesterite (sulfide Cu_2ZnSnS_4 (CZTS), selenide $Cu_2ZnSnSe_4$ (CZTSe), and their alloying $Cu_2ZnSn(S,Se)_4$ (CZTSSe)) thin film solar cells is the large open-circuit voltage deficit ($V_{oc,def}$) issue, which is 0.345 V for the current world record device with an efficiency of 12.6%. In this study, $SnCl_4$ and $SnCl_2{\cdot}2H_2O$ were respectively used as tin precursor to investigate the $V_{oc,def}$ issue of dimethyl sulfoxide (DMSO) solution processed CZTSSe solar cells. Different complexations of tin compounds with thiourea (Tu) and DMSO resulted in different reaction pathways from the solution to the absorber material and thus dramatic differences in photovoltaic performance. The coordination of Sn^{2+} with Tu led to the formation of SnS, ZnS and Cu_2S in the precursor film, which converted to selenides first and then fused to CZTSSe, resulting in poor film quality and device performance. The highest efficiency obtained from this film was 8.84% with a $V_{oc,def}$ of 0.391 V. The coordination of Sn^{4+} with DMSO facilitated direct formation of CZTS phase in the precursor film which directly converted to CZTSSe during selenization, resulting in compositional uniform absorber and high device performance. A device with an active area efficiency of 12.2% and a $V_{oc,def}$ of 0.344 V was achieved from the Sn^{4+} solution processed absorber. Furthermore, CZTSSe/CdS heterojunction heat treatment (JHT) significantly improved the performance of the Sn^{4+} device but had slightly negative effect on the Sn^{2+} device. A champion CZTSSe solar cell with a total area efficiency of 12.4% (active area efficiency of 13.6%) and a low $V_{oc,def}$ of 0.297 V was achieved from the Sn^{4+} solution. Our results demonstrate the preformed uniform CZTSSe phase enabled by Sn^{4+} precursor is the key for the highly efficient CZTSSe absorber. The lowest $V_{oc,def}$ and high efficiency achieved here shines new light on the future of CZTSSe solar cell.**

Keywords: kesterite solar cell, V_{oc} deficit, $SnCl_4$, reaction pathway, heterojunction heat treatment

INTRODUCTION

Kesterite (sulfide, Cu_2ZnSnS_4 (CZTS); selenide, $Cu_2ZnSnSe_4$ (CZTSe); their alloying, $Cu_2ZnSn(S,Se)_4$ (CZTSSe)) semiconductors are promising low-cost photovoltaic absorber materials [1–7], because they have similar theoretical efficiency with the structured copper indium gallium selenide ($Cu(In,Ga)Se_2$, CIGS), yet with less-toxic and earth-abundant elements. However, the efficiency of kesterite solar cell based on CZTSSe absorbers is only 12.6%, which was reported by IBM in 2014 [8] and DGIST in 2019 [9], whereas the efficiency of CIGS solar cell has recently reached 23.35% [10]. The barrier for further improvement of the CZTSSe efficiency is the large open-circuit voltage deficit ($V_{oc,def} = V_{oc}^{SQ} - V_{oc}$, V_{oc}^{SQ} is the maximum achievable V_{oc} based on Shockley-Queisser limit [11]) which is above 0.34 V for the kesterite solar cells but below 0.15 V for CIGS solar cells. Possible reasons for the large $V_{oc,def}$ include potential and band gap fluctuations [12], deep defects [13], recombination at interfaces [14,15], and secondary phases

[1] Key Laboratory for Organic Electronics and Information Displays & Jiangsu Key Laboratory for Biosensors, Institute of Advanced Materials (IAM), Jiangsu National Synergetic Innovation Center for Advanced Materials (SICAM), Nanjing University of Posts & Telecommunications, Nanjing 210023, China
[2] Department of Chemistry, University of Washington, Seattle, WA 98195, USA
[3] Department of Chemical Engineering, University of Washington, Seattle, WA 98195, USA
* Corresponding author (email: iamhxin@njupt.edu.cn)

[16]. Improving V_{oc} is vital for the practical application of CZTSSe solar cells [17,18]. Recent efforts on addressing the $V_{oc,def}$ issue are mainly focused on extrinsic doping [2,19] or alloying [3,11,20,21]. However, none of the reported doping or alloying strategies has led to efficiency higher than the current world record, indicating the optoelectronic properties of CZTSSe absorbers are more likely governed by the intrinsic defects [6,22].

The absorber materials of chalcogenide (CIGS and CZTSSe) thin film solar cells are fabricated from vacuum [4,10,23] or solution [24–28] deposited precursor films by reacting with S, H_2S, Se, H_2Se or a mixture of them (so called sulfurization and selenization) to facilitate grain growth. The property of the absorber material and the photovoltaic performance of the solar cells highly depend on the composition of the precursor film and the reaction pathway from the precursor to the absorber [9,21]. This should be more significant for CZTSSe because it has two metal elements (Cu and Sn) that have variable oxidation state. Moreover, Sn-related deep defects have been reported to be detrimental to the photovoltaic performance [13,29,30]. Thus, the investigation on how Sn precursor oxidation state affects the reaction path from the precursor film to the absorber material and the photovoltaic performance might be able to provide new insight on CZTSSe solar cells. Surprisingly, to the best of our knowledge, no such study has been reported. Compared with vacuum-based approaches, which mostly use metal [9,23] or stannous sulfide [4] as Sn precursor, solution-based method provides an excellent platform for this investigation, because the oxidation state of Sn can be precisely controlled by using stannous (II) or stannic (IV) salts as Sn precursor.

Some of the previous studies presented 4.1% efficiency of CZTSSe solar cells with the absorber fabricated from dimethyl sulfoxide (DMSO) using $SnCl_2{\cdot}2H_2O$, $Cu(OAc)_2$, $ZnCl_2$, and thiourea (Tu) as precursors [31]. Later, by facilitating complete redox reaction between $SnCl_2{\cdot}2H_2O$ and $Cu(OAc)_2$ ($2Cu^{2+}+Sn^{2+}=2Cu^{+}+Sn^{4+}$), the efficiency of CZTSSe solar cell was improved to 8.3% [25]. The redox reaction was intentional to reduce the content of detrimental Cu^{2+}, but more Sn^{2+} were oxidized to Sn^{4+}, which may also account for the improved performance. The efficiency of the CZTSSe solar cells based on DMSO solution was further improved to beyond 11% by alkali metal ions along with the optimization of fabrication condition [2,19,32]. In the above DMSO solution, the Sn and Cu precursors were both +2 oxidation states ($SnCl_2$, $CuCl_2$ or $Cu(OAc)_2$); even with complete redox reaction between Sn^{2+} and Cu^{2+}, there was still Sn^{2+} in the solution due to the requirement of a copper-poor (Cu:Sn < 2, molar ratio) kesterite composition for better device performance. This means at least two reaction paths (Sn^{2+} and Sn^{4+}) were involved in converting the precursors from the solution to the absorber material.

To investigate the reaction paths of Sn^{2+} and Sn^{4+} and their effects on the photovoltaic performance of kesterite, in this study, we respectively used $SnCl_2{\cdot}2H_2O$ and $SnCl_4$ as tin source and CuCl as copper source (to avoid redox reaction) to prepare Sn^{2+} and Sn^{4+} precursor solution and fabricate CZTSSe solar cells. We found that the two solutions indeed took different reaction pathways from the solution to the absorber film, which resulted in dramatic difference in the photovoltaic performance. A highly crystalline precursor film composed of multiple phases including SnS was formed from the Sn^{2+} solution whereas uniform amorphous kesterite phase without secondary phases was obtained from the Sn^{4+} solution. Although both precursor films converted to high-crystalline absorbers upon selenization, the different reaction pathway led to dramatic difference in film morphology, composition and photovoltaic performance. A maximum active area efficiency of 12.2% with a $V_{oc,def}$ of 0.344 V was obtained from the Sn^{4+} device, which was only 8.84% with a $V_{oc,def}$ of 0.391 V for the Sn^{2+} device. Furthermore, heterojunction heat treatment (JHT) of CZTSSe/CdS significantly improved the Sn^{4+} device performance but had slightly negative effect on the Sn^{2+} device. A champion CZTSSe solar cell with a total area efficiency of 12.4% (active area efficiency of 13.6%) and record low $V_{oc,def}$ of 0.297 V was achieved from the Sn^{4+} solution.

EXPERIMENTAL SECTION

Preparation of the molecular precursor solutions

The precursor solutions were prepared in a glovebox with O_2 and H_2O level below 5 ppm at room temperature. First, CuCl-thiourea (Cu-Tu) solution was made by adding 1.602 g of Tu (99%, Aladdin, recrystallized twice) to a vial containing 4 mL of DMSO (99.8%, J&K) under stirring until completely dissolved, and then 0.582 g of CuCl (99.999%, Alfa) was added to obtain a clear solution. For the Sn^{2+} precursor solution, 0.903 g of $SnCl_2{\cdot}2H_2O$ (99.99%, Aladdin), 0.567 g of $ZnCl_2$ (99.95%, Aladdin) and 3 mL of DMSO were subsequently added to the above CuCl-Tu solution and stirred until completely dissolved. For the Sn^{4+} solution, 1.042 g of $SnCl_4$ (99.99%, Alfa) was added into another vial, and the vial was sealed to prevent the evaporation of $SnCl_4$. Then, 3 mL of DMSO was injected into the vial by a syringe. $SnCl_4$ re-

acted with DMSO violently and formed white precipitate. Then 0.763 g of $Zn(OAc)_2$ (99.99%, Aladdin) was added to the $SnCl_4$-DMSO suspension and stirred until a clear solution formed. This solution was then mixed with CuCl-Tu solution to yield a pale yellow solution. We used $Zn(OAc)_2$ instead of $ZnCl_2$ as Zn source for the Sn^{4+} solution because $SnCl_4$ coordinated with DMSO and formed $Sn(DMSO)_4Cl_4$, which had low solubility in DMSO. The use of $Zn(OAc)_2$ reduced the Cl^- concentration and stabilized the precursor solution.

Fabrication of CZTSSe absorber films

Molybdenum-coated soda-lime glass (MSLG) substrates were cleaned by sequential sonication in acetone and 2-propanol, each for 15 min, and dried under N_2 flow. The precursor film was fabricated in a glovebox with O_2 and H_2O level below 5 ppm. The precursor solution was filtered with 0.8 μm polytetrafluoroethylene filter and spin-coated on the clean MSLG substrate at 1500 rpm for 60 s. The wet film was immediately annealed on a hot plate at 420°C for 2 min. The coating-annealing-cooling cycle was repeated seven times to build up a precursor film with a thickness of ~2 μm. The film was then put into a graphite box with Se tablets (~500 mg) and placed in Rapid Heating furnace tube for selenization. The selenization was performed at 550°C for 20 min with Ar flow rate of 20 sccm.

Fabrication of solar cell devices

The cadmium sulfide buffer layer with a thickness of 40–50 nm was deposited on the CZTSSe by the chemical bath deposition (CBD) method [27]. The samples (MSLG/CZTSSe/CdS) were loaded on a sample holder in the chamber, and during sputtering, the chamber was pumped down to vacuum below 2×10^{-3} Pa. For the samples without JHT, a window layer with 50 nm of i-ZnO and 250 nm indium tin oxide (ITO) was directly deposited on the CdS by radio frequency (RF) sputtering at room temperature. For the samples with heterojunction heat treatment, the sample holder (and samples) was heated to 200°C within 30 min and kept at 200°C for a designed time (2 or 20 h), and then the window layer with 50 nm of i-ZnO and 150 nm ITO were deposited at 200°C right after the JHT. Finally, top contact grids of nickel (50 nm) and aluminum (200 nm) were fabricated in a separate thermal deposition system through a shadow mask. The solar cell area was defined by mechanical scribing for approximately 0.105 cm^2 and the accurate area was individually measured as described in the Supplementary information. ITO sputtered at room temperature has higher resistance than that sputtered at 200°C due to poor crystallinity. To ensure similar conductivity, the ITO layer of the device without JHT was thicker (250 nm) than that of the devices with JHT (150 nm). The thinner ITO had slightly higher transparency than thicker ITO.

Film characterization

X-ray diffraction (XRD) (2θ scan) was collected by a Siemens D5005 X-ray powder diffraction system using Cu Kα (λ = 1.5406 Å) X-ray as the source. The Raman spectra were acquired on a Renishaw in Via microscope using 532 or 785 nm laser diode as the excitation source. The surface morphology and elemental composition of the absorber films were measured on a Hitachi S4800 scanning electron microscope (SEM) using 5 kV for imaging and 15 or 20 kV for energy dispersive X-ray (EDX) spectroscopy. The film composition profiles were acquired by glow discharge optical emission spectroscopy (GDOES) using a Horiba GD-Profiler 2 instrument with an anode of 4 mm. Photoluminescence (PL) spectra were acquired on a modified Horiba LabRAM HR-800 using a 785 nm laser diode as the excitation source and a liquid nitrogen-cooled InGaAs array as the detector.

Device characterization

The current density-voltage (*J-V*) curves were measured using a Keithley 2400 Source Meter under simulated AM 1.5 sunlight at 100 mW cm^{-2} irradiance generated by an AAA sun simulator (CROWNTECH, Inc.). The light intensity was calibrated by an NREL-calibrated Si reference cell. The external quantum efficiency (EQE) of the solar cells was measured on Enlitech QE-R3018 using calibrated Si and Ge diodes (Enli technology Co. Ltd.) as references.

RESULTS AND DISCUSSION

Fig. 1a, b show the active area current density-voltage (*J-V*) and EQE curves of the best Sn^{2+} and Sn^{4+} devices fabricated under standard condition with 98 nm MgF_2 antireflective coating (ARC). The device structure and a representative cross-section SEM image of the Sn^{4+} solar cells are shown in Fig. 1c. Since our devices have larger grids (~10.5% total area) than the ideal condition (~4%) due to the mask design and grid fabrication condition, we used active area efficiency to better reflect the absorber property and total area efficiency for fair comparison with the literature, specified throughout the report. The calculation method for the device total and active area is given in Fig. S1. A maximum active area power conver-

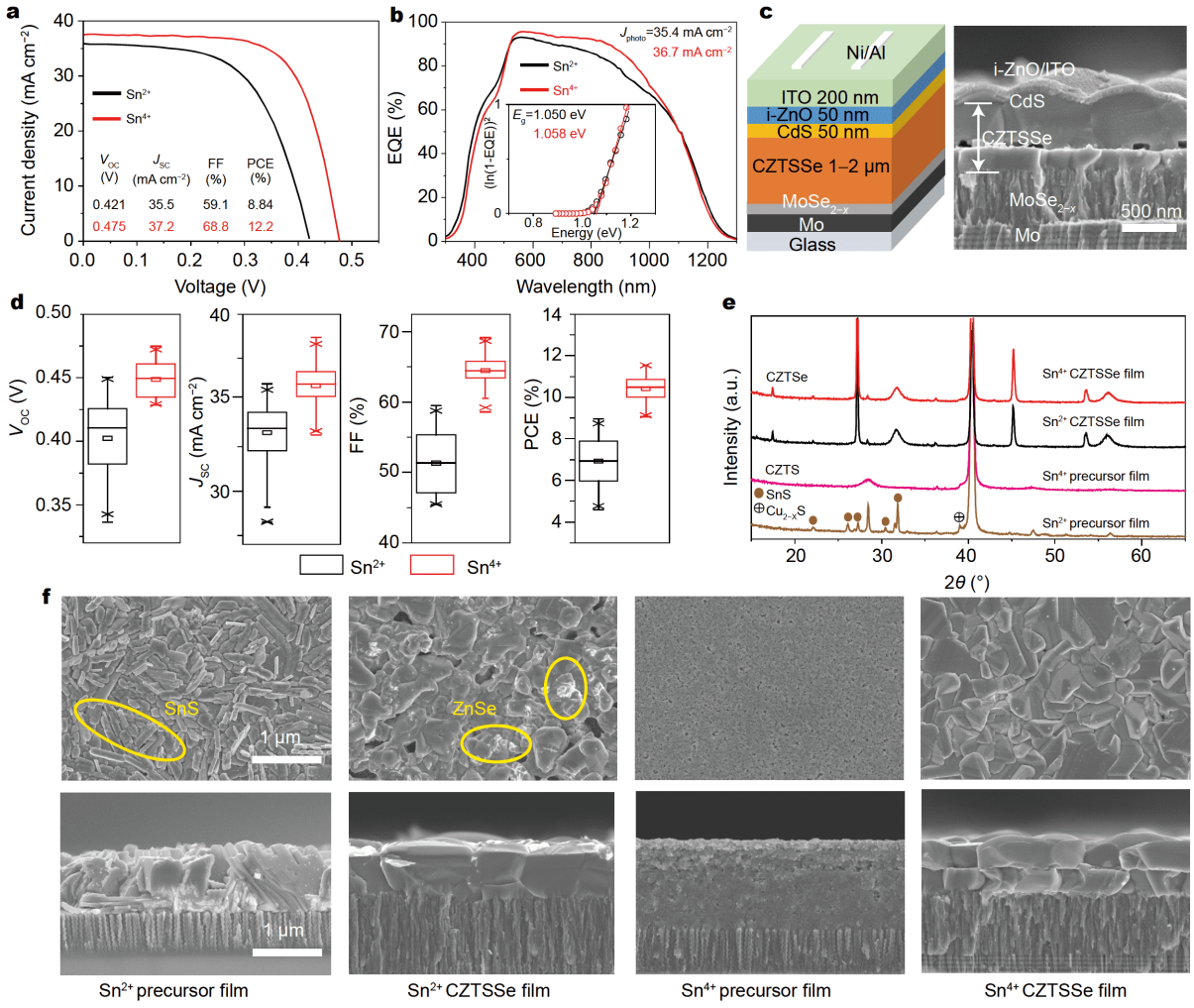

Figure 1 Characterization of the CZTSSe devices and absorber films fabricated from the Sn^{2+} and Sn^{4+} solutions. (a) *J-V* curves, (b) EQE spectra, (c) device structure, (d) statistical photovoltaic parameters, (e) XRD patterns, (f) plane view and cross-section SEM images of the precursor and absorber (CZTSSe) films. All images have the same scale. Inset of (b): bandgap estimation by fitting the expected linear region of the EQE. Data in (d) are from 150 devices for each condition. Devices in (a) have 98 nm MgF_2 ARC. All efficiencies are based on the active area.

sion efficiency (PCE) of 12.2% with short-circuit current density (J_{sc}), V_{oc}, and fill factor (FF) of 37.2 mA cm^{-2}, 0.475 V and 68.8% was achieved by the device based on the Sn^{4+} solution. The PCE, J_{sc}, V_{oc}, FF obtained from the device based on the Sn^{2+} solution were 8.84%, 35.5 mA cm^{-2}, 0.421 V and 59.1%, respectively. The Sn^{4+} solar cells not only have higher value in all device parameters than the Sn^{2+} ones but also exhibit much smaller scattering in all device parameters (Fig. 1d and Table S1), revealing higher quality and uniformity of the Sn^{4+} absorber. The PL spectra (Fig. S2) show that the Sn^{4+} absorber exhibits higher PL intensity, higher peak energy and narrower full width at the half maximum (FWHM) than the Sn^{2+} film. The EQE spectra (Fig. 1b) reveal the Sn^{4+} device has better carrier collection efficiency than the Sn^{2+} device, especially in the near infrared range. The bandgaps of the CZTSSe absorber materials estimated from the EQE data (Fig. 1b, inset) are 1.050 eV for the Sn^{2+} device and 1.058 eV for the Sn^{4+} device. Based on the V_{oc}^{SQ} calculated from equation $V_{oc}^{SQ} = 0.932 \times E_g - 0.167$, the $V_{oc,def}$ of the Sn^{2+} and Sn^{4+} devices are 0.391 and 0.344 V, respectively. A $V_{oc,def}$ of 0.344 V is one of the lowest value achieved from kesterite without extra modification such as doping [6,22], grain boundary passivation [33], or alloying [6,22], demonstrating the priority of the Sn^{4+} precursor in achieving high-quality kesterite absorber.

Fig. 1e shows the powder XRD patterns of the pre-

cursor and absorber films fabricated parallel to the best performing devices in Fig. 1a. For the Sn^{2+} precursor film, sharp diffraction peaks that can be assigned to kesterite Cu_2ZnSnS_4 (PDF# 26-0575) and SnS (PDF#39-0354) are observed together with the detectable peak from $Cu_{2-x}S$ (Fig. 1e). The formation of SnS and $Cu_{2-x}S$ suggests the existence of ZnS because of the Zn-rich composition, although ZnS cannot be distinguished from CZTS due to diffraction peak overlap. The high crystallinity of Sn^{2+} precursor film is also confirmed by SEM (Fig. 1f) and Raman (Fig. S3). In contrast, the Sn^{4+} precursor film only contains amorphous Cu_2ZnSnS_4 as revealed by XRD (Fig. 1e) and Raman (Fig. S3). Both precursor films converted to high crystalline absorber film upon selenization with different morphology (Fig. 1f and Fig. S4). The Sn^{2+} absorber contains large grains with some small grains at the bottom, whereas the Sn^{4+} absorber exhibits a clear double-layer structure with both layers consisting of well-packed large grains. In addition, ZnSe aggregates are observed on the surface of the Sn^{2+} absorber shown in the SEM image (Fig. 1f), whereas the surface of the Sn^{4+} film is clean. Note that a tri-layer structure with a fine-grain middle layer is often observed for the Sn^{4+} films (Fig. S4b), which achieves similar efficiency as the double-layer film, whereas loosely packed small grains are frequently seen for the Sn^{2+} films (Fig. S4a). Further optimizing film fabrication condition to avoid the double-layer morphology is expected to further improve the performance of the Sn^{4+} device. From the EDX spectroscopy measurement (Table S2), both the Sn^{2+} and Sn^{4+} absorber films have a global Cu-poor and Zn-rich composition with Cu:Zn:Sn ratios of 1:0.71:0.62 for the Sn^{2+} absorber and 1:0.71:0.65 for the Sn^{4+} absorber. Compared with the feed-in composition (Cu:Zn:Sn=1:0.68:0.65), the Sn^{2+} film exhibits slight Sn loss.

The solution chemistry and reaction pathways from the solution to the absorber film were investigated to reveal the morphology and performance difference between Sn^{2+} and Sn^{4+} absorbers (Figs S5 and S6). The solution chemistry shows that CuCl, $ZnCl_2$ and $SnCl_2$ coordinate with Tu and form $Cu(Tu)_3Cl$, $Zn(Tu)_2Cl_2$ and $Sn(Tu)_2Cl_2$, which respectively decomposes to $Cu_{2-x}S$, ZnS and SnS upon thermal annealing (Fig. S5). However, $SnCl_4$ only coordinates with DMSO and forms $Sn(DMSO)_4Cl_4$. Annealing a wet film containing $SnCl_4$ and Tu does not form SnS_2 due to the direct decomposition of $Sn(DMSO)_4Cl_4$ to volatile $SnCl_4$ (boiling point 114.15°C). The investigation on the grain growth from precursor film to absorber material (Fig. S7) reveals the amorphous CZTS in Sn^{4+} precursor film directly converts to CZTSSe by substitution reaction at the very early stage of selenization, whereas sulfides $Cu_{2-x}S$, ZnS and SnS in Sn^{2+} precursor film transfer to selenides $Cu_{2-x}Se$, ZnSe, and $SnSe_2$ first before converting to CZTSSe (more detailed grain growth mechanism of the two films will be reported in another paper). Thus, the reaction paths from the Sn^{2+} and Sn^{4+} solutions to the CZTSSe absorbers can be written as follow:

Sn^{2+} solution:

$$CuCl+ZnCl_2+SnCl_2+Tu\rightarrow Cu(Tu)_3Cl+Zn(Tu)_2Cl_2+Sn(Tu)_2Cl_2, \quad (1)$$

$$Cu(Tu)_3Cl+Zn(Tu)_2Cl_2+Sn(Tu)_2Cl_2\rightarrow Cu_2ZnSnS_4+Cu_{2-x}S+ZnS+SnS, \quad (2)$$

$$SnS+Cu_{2-x}S+ZnS+Se\rightarrow SnSe_2+Cu_{2-x}Se+ZnSe, \quad (3)$$

$$SnSe_2+Cu_{2-x}Se+ZnSe\rightarrow Cu_2ZnSnSe_4, \quad (4)$$

$$Cu_2ZnSnS_4+Se\rightarrow Cu_2ZnSn(S,Se)_4. \quad (5)$$

Sn^{4+} solution:

$$CuCl+Zn(OAc)_2+SnCl_4+Tu+DMSO\rightarrow Cu(Tu)_3Cl+Zn(Tu)_2(OAc)_2+Sn(DMSO)_4Cl_4, \quad (6)$$

$$Cu(Tu)_3Cl+Zn(Tu)_2(OAc)_2+Sn(DMSO)_4Cl_4\rightarrow Cu_2ZnSnS_4, \quad (7)$$

$$Cu_2ZnSnS_4+Se\rightarrow Cu_2ZnSn(S,Se)_4. \quad (8)$$

Yang *et al.* [34] reported that the formation of defects is directly correlated to the existence of secondary phases and deep defects can be suppressed by reducing the film inhomogeneity. The co-existence of all three binaries in the Sn^{2+} film during grain growth explains the poor uniformity and low device performance of the Sn^{2+} absorber. In contrast, the direct conversion from CZTS to CZTSe (Fig. S7) enables the compositional and morphological uniformity of the Sn^{4+} absorber and thus superior device performance.

It has been reported that annealing kesterite absorber at low temperature for long time can reduce the Cu-Zn disorder and improve the absorber electronic property [35]. Recently, Yan *et al.* [4] reported that JHT can reduce the interface recombination and improve CZTS solar cell efficiency. We performed the JHT of CdS/CZTSSe at 200° C for 20 h in vacuum. The *J-V* curves of the Sn^{2+} and Sn^{4+} devices with and without JHT are shown in Fig. 2a and their photovoltaic parameters are summarized in Table S3. For the Sn^{2+} device, JHT only slightly increases V_{oc} but decreases J_{sc} and FF, resulting in slightly lower PCE. For the Sn^{4+} device, on the contrary, JHT significantly improves V_{oc} and FF but slightly reduces J_{sc}. The best-performing device with an active area efficiency of 13.0% (without ARC) was achieved from the device based on the Sn^{4+} absorber with J_{sc} of 35.1 mA cm^{-2}, V_{oc} of 0.513 V, and FF of 72.5% (Fig. 2a). The $V_{oc,def}$ of this device is 0.317 V according to the bandgap of 1.070 eV extracted

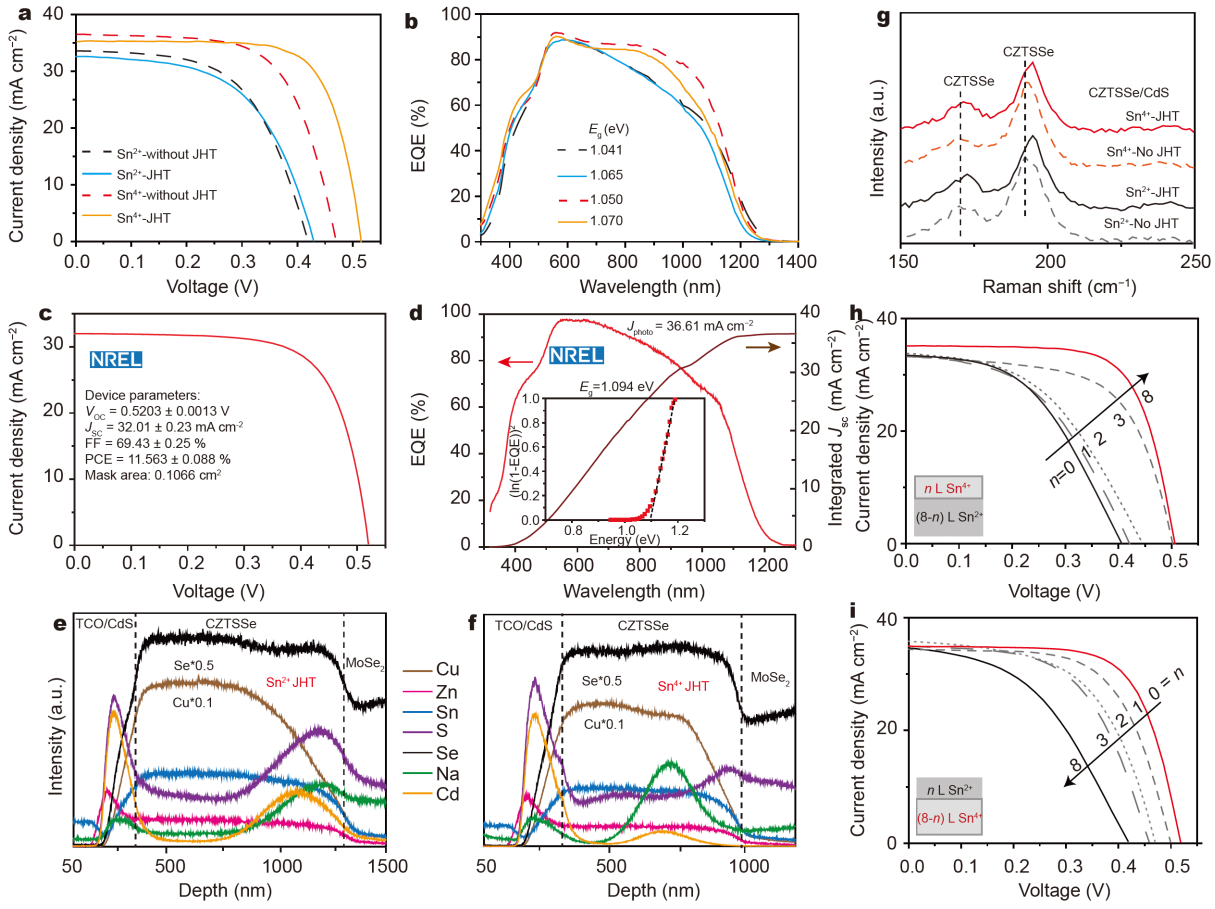

Figure 2 Effect of JHT on device performance. (a) *J-V* curves of the Sn^{2+} and Sn^{4+} solar cells with and without JHT (no ARC). (b) EQE spectra of solar cells in (a). (c) The *J-V* and (d) the EQE of the NREL certified Sn^{4+} device. (e, f) Depth compositional profiles of JHTed Sn^{2+} (e) and Sn^{4+} (f) devices measured by GDOES. (g) Raman spectra of the CdS/CZTSSe films with and without JHT (785 nm laser excitation). (h, i) *J-V* characteristics of the devices with bottom Sn^{2+} and top Sn^{4+} layers (h) and bottom Sn^{4+} and top Sn^{2+} layers (i). The JHT was performed in vacuum for 20 h.

from the EQE (Fig. S8). The statistical data of 150 JHTed devices for 20 h (Fig. S9 and Table S4, active area) show exactly the same trend as Fig. 2a with the average J_{sc}, V_{oc}, FF and PCE of 34.7 mA cm^{-2}, 0.509 V, 70.7%, and 12.5% respectively for the Sn^{4+} devices, which again demonstrate the high reproducibility of the Sn^{4+} absorber.

One of the 20 h-JHTed high performance device with 98 nm MgF_2 ARC was independently measured by NREL and a total area efficiency of 11.56% with J_{sc} of 32.01 mA cm^{-2}, V_{oc} of 0.520 V and FF of 69.43% was certified on an area of 0.1066 cm^2 (Fig. 2c and Fig. S10c). The certified solar cell has an active area efficiency of 13.12% measured in house by excluding the grid area (Fig. S10d). The J_{sc} integrated from the NREL measured EQE (Fig. 2d) is 36.61 mA cm^{-2}, corresponding to an even higher active area efficiency of 13.22%. The $V_{oc,def}$ of the certified device is 0.332 V based on the bandgap of 1.094 eV (Fig. 2d), smaller than that of IBM (0.373 V) [8] and DGIST (0.345 V) [9] record devices.

From Yan *et al.* [4], JHT leads to partial substitution of Zn by Cd which decreases the absorber bandgap and increases the device J_{sc}. Su *et al.* [20] also reported band gap decrease of kesterite with Cd alloying. Glow discharge optical emission spectroscopy (GDOES, Fig. 2e, f) shows both Sn^{2+} and Sn^{4+} absorber films have similar bulk compositional profiles with a large amount of Cd detected. However, the bandgap of our JHTed absorbers increases from 1.041 to 1.065 eV for the Sn^{2+} absorber and 1.050 to 1.070 eV for the Sn^{4+} absorber, indicating different mechanisms. Raman data (Fig. 2g) clearly show a blue-shift of the CZTSSe peaks upon JHT, which is the direct evidence of improvement in kesterite disorder-order [35], thus, the increase of the bandgap can be explained by the improvement in the absorber order-

disorder. To verify how much the order-disorder contributes to the V_{oc} enhancement, annealing absorber film without CdS was conducted under the same condition (at 200°C for 20 h), which only improved the V_{oc} by 16 mV (Fig. S11). The results indicate the order-disorder is not the vital issue for the large $V_{oc,def}$ of kesterite solar cells, in agreement with Rey's report [36].

The similar Cd diffusion, band gap increase and J_{sc} response of the Sn^{2+} and Sn^{4+} absorbers upon JHT indicate JHT has similar effect on the bulk absorber. The difference of JHT on device performance, that is, large improvement in V_{oc} and FF for the Sn^{4+} device but slightly negative effect on the Sn^{2+} device, should come from the surface property of the absorber. From the reaction pathways discussed above, the single phase and direct conversion of kesterite phase for the Sn^{4+} film ensure the uniform composition and thus less-defect surface. For the Sn^{2+} film, on the contrary, the existence of multiphase throughout the grain growth (Fig. S8) inevitably creates high concentration of defects at the surface. To further confirm this, devices with different top and bottom precursor layers (top Sn^{4+}/bottom Sn^{2+} or top Sn^{2+}/bottom Sn^{4+}) were fabricated with their *J-V* characteristics shown in Fig. 2h, i. As expected, the V_{oc} of the devices with top Sn^{4+} layers gradually increases with the increase of the Sn^{4+} layers and reaches that of pure Sn^{4+} device at 3 layers (Fig. 2h and Table S5), whereas the devices with top Sn^{2+} layers display linear decrease of V_{oc} with the increase of Sn^{2+} layers (Fig. 2i and Table S6). In addition, the devices with Sn^{4+} bottom layers have much higher FF than Sn^{2+} bottom layer devices, further confirming the high quality of the Sn^{4+} absorber materials. Further understanding on the mechanism of how JHT affects the CZTSSe/CdS interface property of Sn^{4+}- and Sn^{2+}-based CZTSSe absorber is expected to provide more insight on the limiting factor of kesterite V_{oc}, which is under investigation and will be reported in the future.

The performance improvement of the CZTS solar cell upon JHT was attributed to cation diffusion between CdS and CZTS and the JHT was conducted for a very short time [4]. We suspect the J_{sc} decrease in the 20 h-JHTed devices comes from the deterioration of the absorber bulk property due to long-time heat treatment at the presence of Cd. To confirm this, JHT of 2 h and 20 h were carried out on both Sn^{2+} and Sn^{4+} films, as shown in Fig. S12 and Table S7. As expected, 2 h-JHT results in better performance than 20 h-JHT for both Sn^{2+} and Sn^{4+} devices. For the Sn^{2+} devices, the enhancement is mainly in J_{sc}, whereas both J_{sc} and FF are improved for the Sn^{4+} devices. A champion device with a total area efficiency of 12.4% (no ARC) with J_{sc}, V_{oc}, FF of 33.32 mA cm^{-2}, 0.522 V and 71.5% was achieved from the Sn^{4+} solution. The *J-V* and EQE characteristics of this device are shown in Fig. 3. After excluding the grid area, this device has a J_{sc} of 36.36 mA cm^{-2} (Fig. 3a, dashed line), in excellent agreement with the J_{sc} (36.45 mA cm^{-2}) integrated from the EQE, which corresponds to an active area efficiency of 13.6%. The band gap of this device extracted from the EQE is 1.058 eV. The $V_{oc,def}$ and V_{oc}/V_{oc}^{SQ} of this device are 0.297 V and 63.7%, respectively. To our best knowledge, they are the lowest $V_{oc,def}$ and highest V_{oc}/V_{oc}^{SQ} among all the reported kesterite solar cells.

CONCLUSIONS

In conclusion, we used $SnCl_4$ and $SnCl_2{\cdot}2H_2O$ as tin precursor to investigate the effect of tin oxidation state on DMSO solution-processed kesterite absorber property and solar cell performance. The coordination of Sn^{2+} with Tu leads to a high crystalline precursor film containing SnS, ZnS and $Cu_{2-x}S$, whereas the coordination of Sn^{4+}

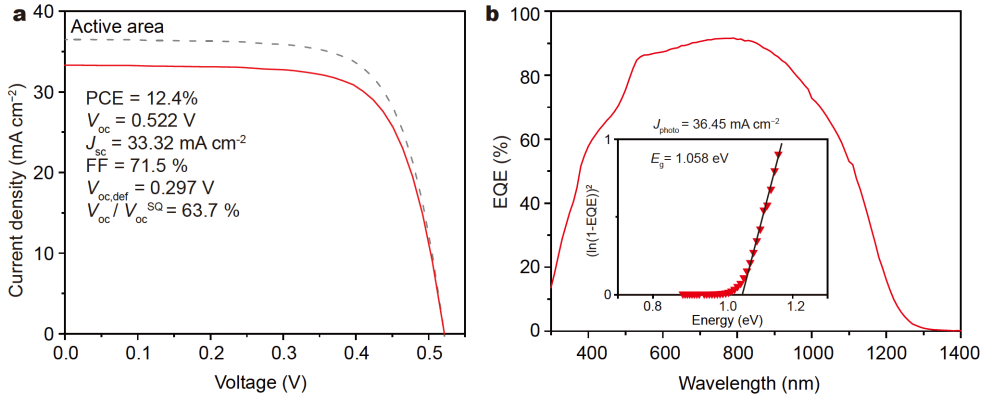

Figure 3 (a) *J-V* and (b) EQE of the champion CZTSSe device fabricated from the Sn^{4+} precursor solution with 2 h JHT.

with DMSO results in direct formation of uniform amorphous kesterite phase. Although both precursor films convert to crystalline CZTSSe absorber upon selenization, the Sn^{2+} film undergoes conversion of multiphase sulfides to selenides and then fusion of selenides to kesterite, resulting in poor absorber with non-uniform composition. In contrast, direct conversion from sulfide to selenide kesterite ensures high-quality absorber material for the Sn^{4+} film. An active area efficiency of 12.2% with V_{oc} of 0.475 V was achieved from the Sn^{4+} device which was only 8.84% with V_{oc} of 0.421 V for the Sn^{2+} device. Furthermore, JHT greatly improves the Sn^{4+} device performance, but has slight negative effect on the Sn^{2+} device. A champion device with a total area efficiency of 12.4% (without ARC), active area efficiency of 13.6%, lowest $V_{oc,def}$ of 0.297 V, and highest V_{oc}/V_{oc}^{SQ} of 63.7% has been achieved from the kesterite absorber fabricated from DMSO solution using Sn^{4+} precursor. Our results demonstrate a preformed uniform kesterite phase (as the Sn^{4+} precursor film in this report) is critical to ensure high-quality absorber materials, whereas the fusion of multi secondary phases (as the Sn^{2+} precursor film in this report and most cases in the literature due to the starting precursors are metal or/and binary sulfides) creates defects due to the existence of secondary phases. Our finding provides a new platform and direction for investigating the mechanism of the $V_{oc,def}$ issue of kesterite and further improving kesterite solar cell efficiency.

Received 13 May 2020; accepted 20 May 2020; published online 29 July 2020

1 Todorov TK, Tang J, Bag S, *et al.* Beyond 11% efficiency: Characteristics of state-of-the-art $Cu_2ZnSn(S,Se)_4$ solar cells. Adv Energy Mater, 2013, 3: 34–38
2 Xin H, Vorpahl SM, Collord AD, *et al.* Lithium-doping inverts the nanoscale electric field at the grain boundaries in $Cu_2ZnSn(S,Se)_4$ and increases photovoltaic efficiency. Phys Chem Chem Phys, 2015, 17: 23859–23866
3 Qi YF, Kou DX, Zhou WH, *et al.* Engineering of interface band bending and defects elimination *via* a Ag-graded active layer for efficient $(Cu,Ag)_2ZnSn(S,Se)_4$ solar cells. Energy Environ Sci, 2017, 10: 2401–2410
4 Yan C, Huang J, Sun K, *et al.* Cu_2ZnSnS_4 solar cells with over 10% power conversion efficiency enabled by heterojunction heat treatment. Nat Energy, 2018, 3: 764–772
5 Guo L, Shi J, Yu Q, *et al.* Coordination engineering of Cu-Zn-Sn-S aqueous precursor for efficient kesterite solar cells. Sci Bull, 2020, 65: 738–746
6 Giraldo S, Jehl Z, Placidi M, *et al.* Progress and perspectives of thin film kesterite photovoltaic technology: A critical review. Adv Mater, 2019, 31: 1806692
7 Liu F, Wu S, Zhang Y, *et al.* Advances in kesterite $Cu_2ZnSn(S, Se)_4$ solar cells. Sci Bull, 2020, 65: 698–701
8 Wang W, Winkler MT, Gunawan O, *et al.* Device characteristics of CZTSSe thin-film solar cells with 12.6% efficiency. Adv Energy Mater, 2014, 4: 1301465
9 Son DH, Kim SH, Kim SY, *et al.* Effect of solid-H_2S gas reactions on CZTSSe thin film growth and photovoltaic properties of a 12.62% efficiency device. J Mater Chem A, 2019, 7: 25279–25289
10 Nakamura M, Yamaguchi K, Kimoto Y, *et al.* Cd-free $Cu(In,Ga)(Se,S)_2$ thin-film solar cell with record efficiency of 23.35%. IEEE J Photovoltaics, 2019, 9: 1863–1867
11 Collord AD, Hillhouse HW. Germanium alloyed kesterite solar cells with low voltage deficits. Chem Mater, 2016, 28: 2067–2073
12 Hadke S, Levcenko S, Sai Gautam G, *et al.* Suppressed deep traps and bandgap fluctuations in Cu_2CdSnS_4 solar cells with ≈8% efficiency. Adv Energy Mater, 2019, 9: 1902509
13 Chen S, Walsh A, Gong XG, *et al.* Classification of lattice defects in the kesterite Cu_2ZnSnS_4 and $Cu_2ZnSnSe_4$ earth-abundant solar cell absorbers. Adv Mater, 2013, 25: 1522–1539
14 Gunawan O, Todorov TK, Mitzi DB. Loss mechanisms in hydrazine-processed $Cu_2ZnSn(Se,S)_4$ solar cells. Appl Phys Lett, 2010, 97: 233506
15 Min X, Guo L, Yu Q, *et al.* Enhancing back interfacial contact by *in-situ* prepared MoO_3 thin layer for $Cu_2ZnSnS_xSe_{4-x}$ solar cells. Sci China Mater, 2019, 62: 797–802
16 Kumar M, Dubey A, Adhikari N, *et al.* Strategic review of secondary phases, defects and defect-complexes in kesterite CZTS–Se solar cells. Energy Environ Sci, 2015, 8: 3134–3159
17 Antunez PD, Bishop DM, Luo Y, *et al.* Efficient kesterite solar cells with high open-circuit voltage for applications in powering distributed devices. Nat Energy, 2017, 2: 884–890
18 Siebentritt S. High voltage, please! Nat Energy, 2017, 2: 840–841
19 Haass SG, Andres C, Figi R, *et al.* Complex interplay between absorber composition and alkali doping in high-efficiency kesterite solar cells. Adv Energy Mater, 2018, 8: 1701760
20 Su Z, Tan JMR, Li X, *et al.* Cation substitution of solution-processed Cu_2ZnSnS_4 thin film solar cell with over 9% efficiency. Adv Energy Mater, 2015, 5: 1500682
21 Giraldo S, Saucedo E, Neuschitzer M, *et al.* How small amounts of Ge modify the formation pathways and crystallization of kesterites. Energy Environ Sci, 2018, 11: 582–593
22 Romanyuk YE, Haass SG, Giraldo S, *et al.* Doping and alloying of kesterites. J Phys Energy, 2019, 1: 044004
23 Lee YS, Gershon T, Gunawan O, *et al.* $Cu_2ZnSnSe_4$ thin-film solar cells by thermal co-evaporation with 11.6% efficiency and improved minority carrier diffusion length. Adv Energy Mater, 2015, 5: 1401372
24 Todorov T, Hillhouse HW, Aazou S, *et al.* Solution-based synthesis of kesterite thin film semiconductors. J Phys Energy, 2020, 2: 012003
25 Xin H, Katahara JK, Braly IL, *et al.* 8% Efficient $Cu_2ZnSn(S,Se)_4$ solar cells from redox equilibrated simple precursors in DMSO. Adv Energy Mater, 2014, 4: 1301823
26 Fu J, Fu J, Tian Q, *et al.* Tuning the Se content in $Cu_2ZnSn(S, Se)_4$ absorber to achieve 9.7% solar cell efficiency from a thiol/amine-based solution process. ACS Appl Energy Mater, 2018, 1: 594–601
27 Jiang J, Giridharagopal R, Jedlicka E, *et al.* Highly efficient copper-rich chalcopyrite solar cells from DMF molecular solution. Nano Energy, 2020, 69: 104438
28 Wu S, Jiang J, Yu S, *et al.* Over 12% efficient low-bandgap $CuIn(S, Se)_2$ solar cells with the absorber processed from aqueous metal complexes solution in air. Nano Energy, 2019, 62: 818–822

29 Li J, Yuan ZK, Chen S, *et al.* Effective and noneffective recombination center defects in Cu_2ZnSnS_4: Significant difference in carrier capture cross sections. Chem Mater, 2019, 31: 826–833
30 Kim S, Park JS, Walsh A. Identification of killer defects in kesterite thin-film solar cells. ACS Energy Lett, 2018, 3: 496–500
31 Ki W, Hillhouse HW. Earth-abundant element photovoltaics directly from soluble precursors with high yield using a non-toxic solvent. Adv Energy Mater, 2011, 1: 732–735
32 Haass SG, Diethelm M, Werner M, *et al.* 11.2% Efficient solution processed kesterite solar cell with a low voltage deficit. Adv Energy Mater, 2015, 5: 1500712
33 Gershon T, Shin B, Bojarczuk N, *et al.* The role of sodium as a surfactant and suppressor of non-radiative recombination at internal surfaces in Cu_2ZnSnS_4. Adv Energy Mater, 2015, 5: 1400849
34 Yang KJ, Sim JH, Son DH, *et al.* Precursor designs for $Cu_2ZnSn(S, Se)_4$ thin-film solar cells. Nano Energy, 2017, 35: 52–61
35 Rey G, Redinger A, Sendler J, *et al.* The band gap of $Cu_2ZnSnSe_4$: Effect of order-disorder. Appl Phys Lett, 2014, 105: 112106
36 Rey G, Weiss TP, Sendler J, *et al.* Ordering kesterite improves solar cells: A low temperature post-deposition annealing study. Sol Energy Mater Sol Cells, 2016, 151: 131–138

Acknowledgements This work was supported primarily by the National Natural Science Foundation of China (21571106 and U1902218). Jiang J and Yu S acknowledge the support from the Postgraduate Research and Practice Innovation Program of Jiangsu Province. Jedlicka E and Giridharagopal R acknowledge the support from the Molecular Analysis Facility, a National Nanotechnology Coordinated Infrastructure site at the University of Washington which is supported in part by the National Science Foundation (NNCI-1542101), the University of Washington, the Molecular Engineering & Sciences Institute, the Clean Energy Institute, and the National Institutes of Health.

Author contributions Gong Y and Xin H conceived the idea and cowrote the manuscript. Xin H and Huang W supervised this study. Gong Y and Zhang Y fabricated the devices and conducted most of the measurements. Jedlicka E and Giridharagopal R conducted the GDOES measurements and initial data process. Clark J conducted the PL measurements. Niu C, Qiu R, Jiang J, Yu S and Wu S provided assistance in the device fabrication and measurements. Yan W, Huang W, Hillhouse H and Ginger D discussed the results and provided valuable suggestions to the manuscript.

Conflict of interest The authors declare no conflict of interest.

Supplementary information Experimental data and supporting data are available in the online version of the paper.

Yuancai Gong is a PhD candidate in the Institute of Advanced Materials, School of Materials Science and Engineering, Nanjing University of Posts & Telecommunications, under the supervision of Prof. Hao Xin. His research focuses on earth-abundant kesterite thin film solar cells.

Hao Xin is a professor of materials science and engineering at Nanjing University of Posts and Telecommunications. She received her PhD from Peking University in 2003. She was a JST CREST researcher at NIMS and a JSPS fellow at JAIST from 2003 to 2006. Then she worked in the Department of Chemical Engineering at the University of Washington until 2012. Her current research interests are solution processed thin film solar cells including CZTS, CIGS and perovskite.

全面积效率12.4%、开路电压损失低于0.30 V的CZTSSe太阳能电池：Sn^{4+}前驱体在DMSO溶液中的使用

龚元才[1], 张一凡[1], Erin Jedlicka[2], Rajiv Giridharagopal[2], James A. Clark[3], 闫伟博[1], 牛传友[1], 邱瑞婵[1], 江晶晶[1], 余绍棠[1], 吴三平[1], Hugh W. Hillhouse[3], David S. Ginger[2], 黄维[1], 辛颢[1*]

摘要 开路电压损失($V_{oc,def}$)大是制约锌黄锡矿结构CZTSSe太阳能电池效率的关键因素，目前世界纪录效率(12.6%) CZTSSe电池的$V_{oc,def}$为0.345 V. 本文分别以$SnCl_4$和$SnCl_2{\cdot}2H_2O$为锡前驱体研究二甲基亚砜(DMSO)溶液法制备的CZTSSe太阳能电池的开路电压损失问题. 研究发现不同价态的锡前驱体化合物与有机配体硫脲(Tu)和溶剂DMSO发生不同的配位反应，使得从溶液到CZTSSe吸光层薄膜的反应路径截然不同. Sn^{2+}与Tu配位导致前驱体薄膜中SnS、ZnS和Cu_2S的生成，这些硫化物在硒化过程中首先转化成硒化物而后逐步熔合生成CZTSSe，其反应路径中多物相的转化和熔合导致薄膜光电性能差，由该薄膜获得的最优器件有效面积效率仅为8.84%，$V_{oc,def}$ 为0.391 V. 而Sn^{4+}与DMSO配位，该前驱体溶液经退火直接得到组成均匀的CZTS前驱体薄膜，在硒化过程中CZTS直接发生取代反应生成CZTSSe，得到的CZTSSe薄膜组成均匀，光电性能优异，由该薄膜制备的器件有效面积效率达到12.2%，$V_{oc,def}$降低至0.344 V. 此外，CZTSSe薄膜性质的不同导致CZTSSe/CdS异质结热处理(JHT)结果的不同. JHT显著提高了Sn^{4+}器件的性能，却略微降低了Sn^{2+}器件的性能. 最终，由Sn^{4+}溶液获得了全面积效率为12.4%，有效面积效率高达13.6%，$V_{oc,def}$低至0.297 V的CZTSSe太阳能电池器件. 研究结果表明通过控制溶液中化学组成获得组成均匀的CZTS预制膜是获得高效CZTSSe电池薄膜材料和降低器件$V_{oc,def}$的关键. 本报道不仅为进一步提高CZTSSe电池效率提供了新的思路，而且实现了$V_{oc,def}$首次低于0.30 V，预示了CZTSSe未来的应用前景.

